Marie Curie Summer Schools
Knowledge Based materials
Hydrous and Porous Materials
19th-29th August 2008, Trest, Czech Republic

Biomineralization Inspired Material Syntheses

Giuseppe Falini
Biocrystallography and Biomineralization Group
Laboratory of Environmental and Biological Structural Chemistry
Department of Chemistry "G. Ciamician"
Alma Mater Studiorum Università di Bologna
Italy

Nature is the ultimate architect

Biomimetic (or biological inspired synthesis) is the abstraction of good design from Nature. Biological materials are often more efficient in their function than their artificial counterparts. Biomimetic is a multidisciplinary science where ideas from Nature are harnessed by Biologists, Material Scientists, Chemists and Engineers and used to design new "smart" materials or structure to perform specific functions

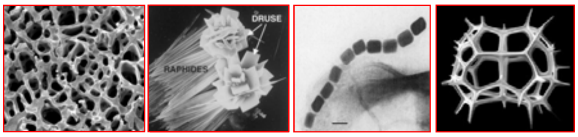

Biomaterials from Biological Inspired Synthetic Strategies

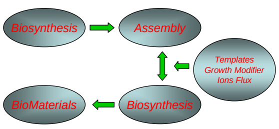

Generalized scheme of biological materials synthesis

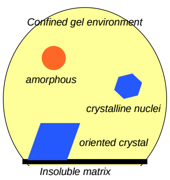

Assembling some ideas . . . .

Biomaterials inspired growth

- **Biosynthesis**
  - **by organisms**
  - **in biological templates**
- **Biotemplating**
  - **on biological structured surfaces**
  - **in assembled monolayers**
  - **in confinements**
  - **gelling environments**

Biomaterials synthesis using bacterial and virus templates

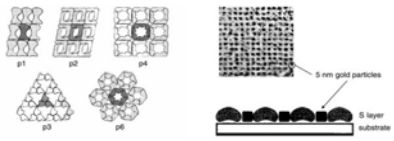

left Bacterial surface layers (S layers). Different types of S layers with a diagonal (p1, p2), square (p4), or hexagonal (p3, p6) symmetry. *right* TEM image of a gold superlattice prepared by using a square S layer lattice mounted on a substrate.

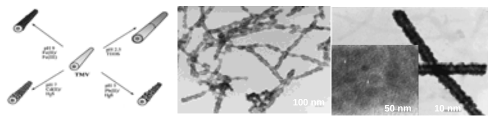

left Scheme showing routes for the synthesis of nanotube composites using tobacco mosaic virus (TMV). *center* TEM images of iron oxide±coated TMV rods. *right* TEM micrographs of CdS-mineralized TMV particles.

U. B. Sleytr, et al. Angew. Chem. Int. Ed. 1999.

Biomaterials synthesis using biological nanoreactor and cells

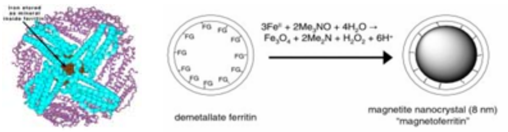

The ferritin hollow protein cages used as spatially confined bioreactors for the growth of inorganic nanoparticles (FG.functional group, which acts as a nucleation site for biomineralization)

Name	Organism	Product	Size	Conditions
Pseudomonas stutzeri	Bacteria	Ag^0	<200 nm	Grown in $AgNO_3$
Medicago sativa	Alfalfa plant	Au^0	2–20 nm	Active uptake Au^0
Pedomicrobium-Like	Budding bacteria	Au^0	~1 µm	Natural mineralization
Verticillium sp.	Fungus	Au^0	20 nm	Intracellular reduction
Verticillium sp.	Fungus	Ag^0	25 nm	Intracellular reduction
Lactobacillus strains	Bacteria (buttermilk)	Au^0	25–50 nm	Exposure to $HAuCl_4$
Lactobacillus strains	Bacteria (buttermilk)	Ag^0	15–500 nm	Exposure to $AgNO_3$
Fusarium oxysporum	Fungus	Au^0	20–40 nm	Extracellular reduction
Cylindrotheca fusiformis	Diatom	SiO_2	500–700 nm	Exposure to $Si(OH)_4$
Coscinodiscus granii	Diatom	SiO_2	Undefined	Exposure to $Si(OH)_4$
Aquaspirillum	Bacteria	Fe_3O_4	25–55 nm	2–7 µM oxygen
A. Magnetotacticum	Bacteria	Fe_3O_4	Undefined	2–7 µM oxygen
Undesignated	Magnetotactic bacteria	Fe_3S_4	69 nm	Anaerobic
Schizosaccharomyces pombe	Yeast	CdS	1.8 nm	Peptide mediated Cd^{2+}
Candida glabrata	Yeast	CdS	2.0 nm	Peptide mediated Cd^{2+}
Fusarium oxysporum	Yeast	CdS	5–20 nm	Extracellular reduction
Klebsiella aerogenes	SO_4^{2-} reducing bacteria	CdS	20–200 nm	Exposure to Cd^{2+}/SO_4^{2-}
Pseudomonas stutzeri	Bacteria	Ag_2S	Undefined	Grown in $AgNO_3$
Desulfobacteriaceae	Bacterial biofilm	ZnS	2–5 nm	pH 7.2–8.6 (0.1 ppm Zn)

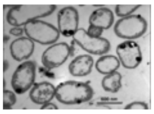

TEM of a thin section of *P. stutzeri* AG259 cells. Crystalline Ag particles deposited between the cell wall and the plasma membrane.

Cells are utilized for the production of nano-particles of metals, metal oxides and metal sulfides

T. Klaus, et al. PNAS, 2003.

Biomaterial synthesis by organisms

Tissue generation - regeneration in the shell

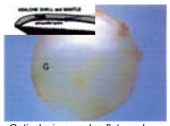

Optical micrograph a flat pearl.

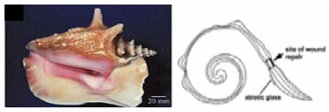

Shell of a wild conch, *Stromgus gigas.*

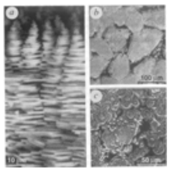

SEM images showing the ultrastructure and the development of "flat pearls"

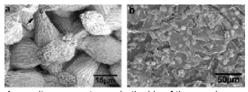

Aragonite aggregates on both side of the membrane.

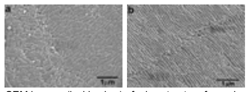

SEM images (inside view) of microstructure formed wound repair and in wild shell

M. Fritz, Nature, 1994; X. Su, Chem. Mater., 2004

MCSS, 19-29 August 2008, Trest

Biomaterial synthesis in biological templates

Ordered macroporous chitin-silica composites

Cuttle bone
Sepia officinalis

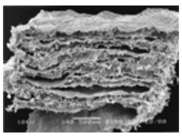

SEM images of β-chitin organic matrix isolated from cuttlebone,

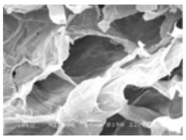

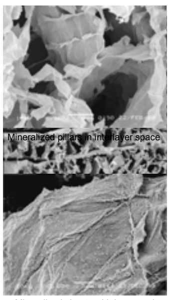

Mineralized sheets with increased silica loading.

Mann et al. Chem. Mat., 2000

MCSS, 19-29 August 2008, Trest

Biomaterial synthesis in biological templates

Aragonite-hydroxyapatite hydrothermal conversion

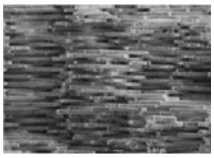

SEM image of a cross section of native gastropod nacre.

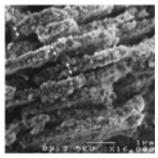

SEM images of cross-section fractures through the bulk of nacre pieces fully converted to HA

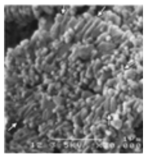

Plan-view tablet of HA-converted nacre,

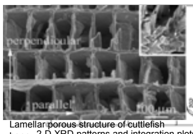

Lamellar porous structure of cuttlefish bone.. 2-D XRD patterns and integration plots over 30 regions in ø (indicated) plotted as intensity versus degrees 2θ

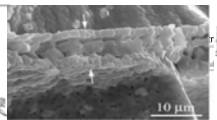

Typical bi-layer features observed at fracture surfaces of scaffolds' walls.

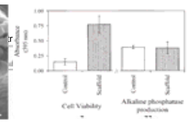

Zaremba et al. Chem. Mat, 1998
Ferreira et al. Biomed. J., 2005

Biomaterial synthesis in biological templates

Calcite single crystal -hydroxyapatite hydrothermal conversion

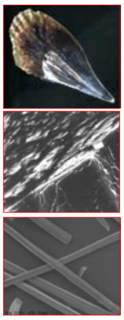

Biogenic single crystals of calcite from the mollusc shell *Atrina rigida*

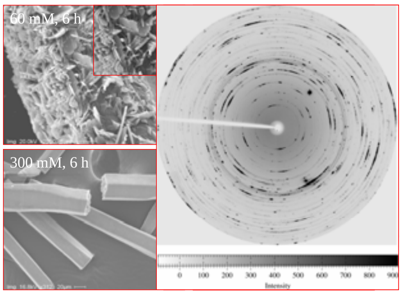

The overall shape of the single crystal is conserved and calcite transformed hydroxyapatite

Falini et al. Chem. Mat, 2008, submitted

Biomaterial synthesis in Langmiur monolayers

Crystallization in self organizing templates

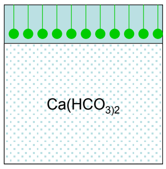

Calcite crystal nucleated under *n*-eicosylsulphate monolayer, and schematic diagram showing orientation of crystal

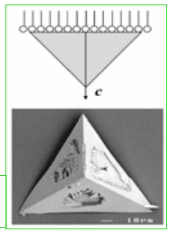

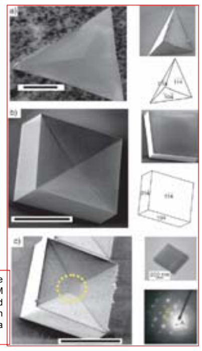

Calcite crystals grown under monolayers a) SEM image observed from the side attached to the monolayer and viewed from the side exposed to the solution. b) SEM image of a rhombohedral crystal with a concave central region from the side attached to the monolayerviewed from the side exposed to the solution. c) SEM image of an indented crystal showing a central patch image and electron diffraction pattern of a rhombohedral crystal.

Biomaterial synthesis on biological structured surfaces

Shaping amorphous calcium carbonate

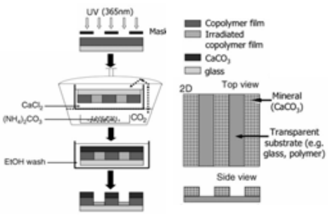

Schematic representation of a 2D model substrate and the experimental procedure for the generation of patterns of $CaCO_3$.

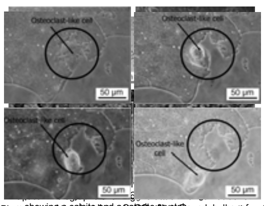

Phase-contrast optical micrographs illustrating a resorption pit on the $CaCO_3$ film and an osteoclast-like cell.

Sommerdijk et al. Angew. Chem. Int. Ed., 2006

MCSS, 19-29 August 2008, Trest

Biomaterial synthesis in self assembled monolayers

Crystallization in patterns

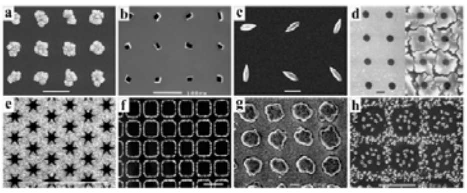

Examples of micropatterned $CaCO_3$ films formed on the SAM templates

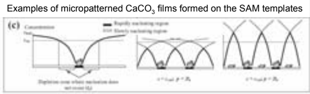

Schematic illustration of the experimental steps for the fabrication of micropatterned substrates used for the crystals growth experiments: a) microcontact printing; b) topographically assisted selfassembly. c) mechanism of localized crystals growth.

Aizenberg et al. Adv. Mat, 2004

MCSS, 19-29 August 2008, Trest

Mineral growth on self assembled monolayers

Crystallization of biomaterials in patterns

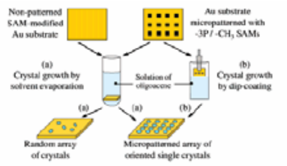

Schematic Illustration of the Experimental Procedure for the SAM-Induced Growth of Organic Semiconductor Crystals from an Oligoacene/THF Solution

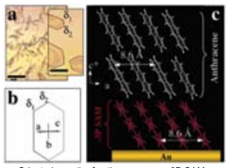

Oriented growth of anthracene on a -3P SAM

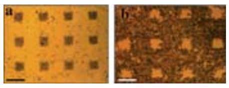

Optical micrographs of patterned arrays of anthracene crystals grown on micropatterned SAMs.

Aizenberg et al. JACS, 2006

Biomaterial synthesis on structured surfaces

$CaCO_3$ precipitation control by means of nanotechnology

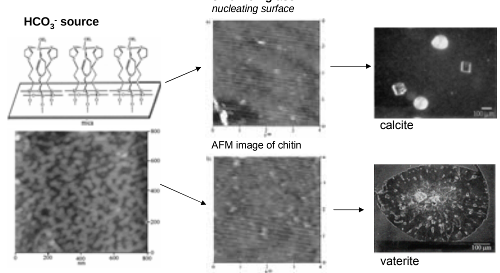

An AFM image of the self-organized ImSi monolayer over mica surface

AFM image of chitin

AFM image of chitin with Pasp

K. Ichikawa et al., *Chem. Eur. J.* 2003.

Biomaterial synthesis on templates

Single crystals in structured polymeric templates

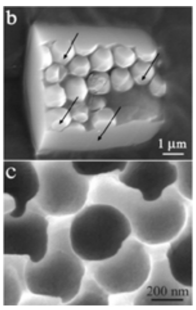

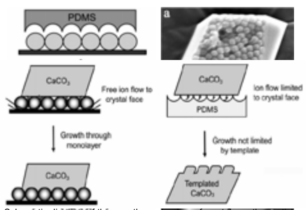

Schematic diagram of the growth mechanism of crystals on the particle monolayers and on the PDMS replica.

Meldrum et al. J.Mat.Chem., 2006

Biomaterial synthesis in confinements

Single crystals in structured polymeric templates

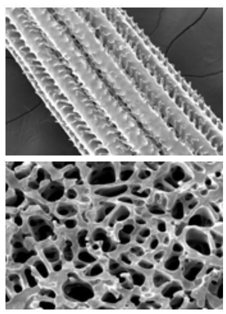

Sea urchin spine

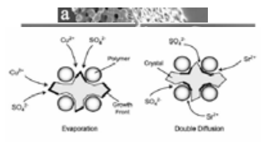

Schematic diagram showing the influence of the precipitation route on the surface structure of the templated particles formed.

a polymer template of sea urchin skeletal plate;
c templated single crystal of calcite precipitated.

Meldrum et al. J.Mat.Chem., 2006

Biomaterial synthesis in confinements

Crystallization of confined in patterns

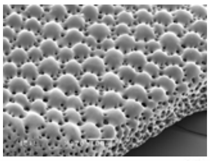

Schematic presentation of the structure of the epidermis and dermis in the DAP. Lenses (L), pigment (P), cuticle of the epidermis (E), epithelial cells (EC) and nerve bundles (N) are indicated.

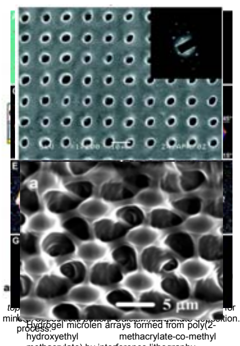

Hydrogel microlen arrays formed from poly(2-hydroxyethyl methacrylate-co-methyl methacrylate) by interference lithography.

Aizenberg et al. Science, 2003

Biomaterial synthesis in confinements

Chitin-silk fibroin substrates

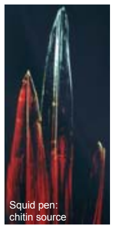

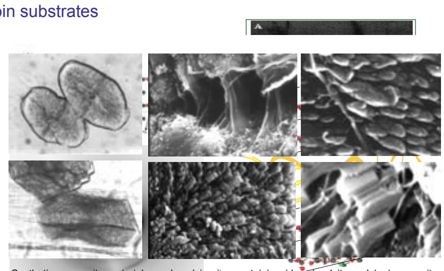

Synthetic composite materials produced *in vitro* containing (down) calcite and (up) aragonite crystals in the matrix. The matrix is composed of β-chitin and silk fibroin, as well as soluble macromolecules extracted from the calcitic and the aragonitic layers of the shell of the *Atrina serrata*

SEM images of chitin-silk fibroin composite film

Samples of chitin, chitin silk fibroin and organic matrix marked with Rhodamine B.

Addadi et al. Conn. Tissue., 2004

Biomaterial synthesis in confinements

Crystallization collagenous substrates

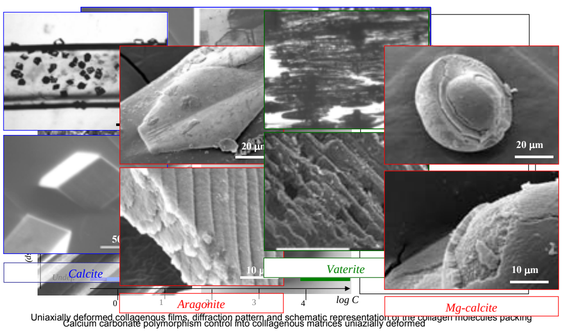

Uniaxially deformed collagenous films, diffraction pattern and schematic representation of the collagen molecules packing

Calcium carbonate polymorphism control into collagenous matrices uniaxially deformed

Falini et al. Dalton Trans., 2001

Biomaterial synthesis in gelling environments

Crystallization of calcium carbonate

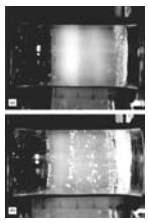

Acrylamide-co-acrylic acid hydrogels as growth medium for $CaCO_3$ in a double-diffusion arrangement after 7 days (a) and 28 days (b) mineralization time.

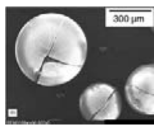

SEM micrograph of a spherulitic particle

SEM micrograph of a spherulitic particle cross section

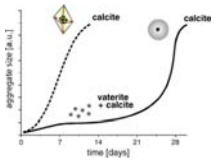

Schematic representation of the course of mineralization in genuine poly-acrylamide gels (broken line, and poly-acrylamide-co-acrylic acid hydrogels (solid line) as a function of time.

O. Grassmann et al. Biomaterials, 2004.

Biomaterial synthesis in structured templates
Nanostructured artificial nacre

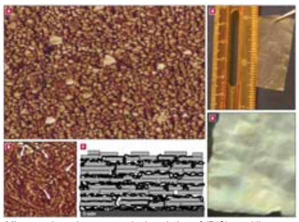

Microscopic and macroscopic description of (P/C)*n* multilayers.

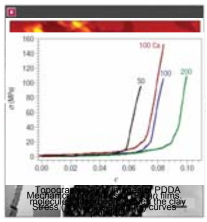

Electron microscopy images of (P/C)*n* multilayers.

Polyelectrolyte folding and P–C ion-pair formation

Biomaterial synthesis in gelling environments
Apatite crystal growth in an amelogenin-rich matrix

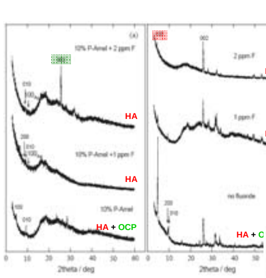

XRD patterns of the products grown on the membrane

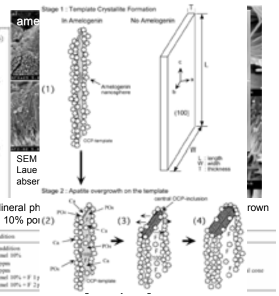

Schematic representation of the proposed functions of amelogenin nanospheres and fluoride in regulating the mineral phase, habit and size of the crystals.

Biomaterial synthesis on structured surfaces
Apatite crystal growth in an amelogenin-rich matrix

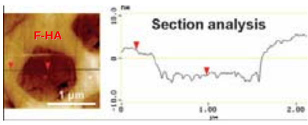

AFM-image of glass-ceramic substrate after polishing and before immersion into mineralizing solutions.

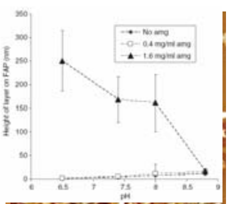

Graph comparing the height of the mineralized layer formed on FAP crystals at different pHs and protein concentrations.

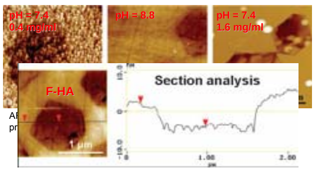

AFM-image of glass-ceramic substrate after polishing and before immersion into mineralizing solutions.

The value of biological control… from materials assembly ….to Bolognese cousine

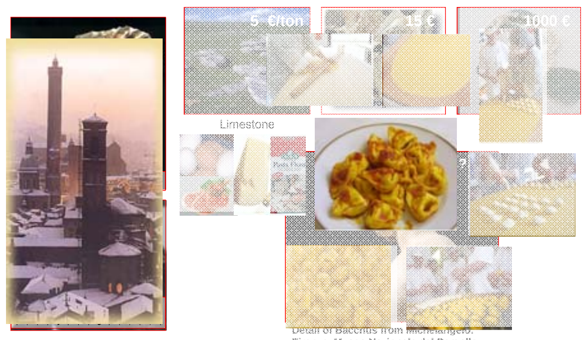

from biomaterials synthesis ….to toothpaste